Coverage Analysis for the Core/Shell Electrode of Dye-Sensitized Solar Cells

Ta-Chang Tien,*,† Fu-Ming Pan,*,† Lih-Ping Wang,‡ Feng-Yu Tsai,§ and Ching Lin§

Department of Material Science and Engineering, National Chiao Tung University, Taiwan, 300, ROC, Photovoltaics Technology Center and Nanotechnology Research Center, Industrial Technology Research Institute, Taiwan, 310, ROC, and Department of Materials Science and Engineering, National Taiwan University, Taiwan, 106, ROC

Received: March 15, 2010; Revised Manuscript Received: April 16, 2010

In this study, we established a core/shell (C/S) model that evaluates the surface coverage of an overlayer deposited on nanoparticles in terms of X-ray photoelectron spectroscopy signals of the nanoparticles. We used the model to estimate the coverage of Al_2O_3 shell layers, which were deposited on the nanoporous TiO_2 electrodes of dye-sensitized solar cells (DSSCs) by atomic layer deposition (ALD), as a function of the number of ALD reaction cycles. The surface coverage increased with the average thickness of the Al_2O_3 shell layers, indicating that the ALD Al_2O_3 deposition on the nanoporous electrode was via the island growth mode. The power conversion efficiency of the DSSCs was highest after the first ALD reaction cycle for the Al_2O_3 shell layers, which had a coverage of 0.25, according to the C/S model. The study shows that, to further improve the PCE, optimization of the ALD Al_2O_3 deposition condition is required so that the surface coverage of the shell layer can be increased at the first ALD reaction cycle.

I. Introduction

Nanoporous materials possessing core/shell (C/S) structures are attracting great interest because of their promising application in catalysis, sensors, batteries, fuel cells, and solar cells.[1−5] Among the most popular of these applications, dye-sensitized solar cells (DSSCs) based on nanoporous electrodes comprising interconnected TiO_2 nanoparticles exhibit an enhancement (by 10−35%) in the power conversion efficiency (PCE) when Al_2O_3 shell layers cap on TiO_2 nanoparticles.[6−8] The improved performance of DSSCs featuring Al_2O_3 shell layers is based on decreases in the degrees of charge recombination and electron transfer from the dye through the Al_2O_3 overlayers via a tunneling effect.[9−13] The increased PCE of dye-sensitized TiO_2 solar cells featuring Al_2O_3 shell layers with an optimal thickness is related to their interfacial energy levels, that is, the high recombination energy barrier of the Al_2O_3−TiO_2 interface, the high work function of the Al_2O_3 overlayers, and the low energy barrier between the dye and Al_2O_3. Optimization of the Al_2O_3−TiO_2 interface in DSSCs can be performed using different coating procedures, which so far have relied on the good coverage of the shell layer of the nanoporous electrode. Atomic layer deposition (ALD) is usually considered an ideal method to deposit ultrathin films of high uniformity and conformity and, therefore, is presumed to be able to achieve an excellent PCE enhancement when it is used to coat the Al_2O_3 shell layer on nanoporous TiO_2 electrodes. However, in a previous study,[14] we found that the PCE enhancement for our DSSCs featuring the ALD Al_2O_3 shell layers is not better than that for DSSCs with Al_2O_3 shell layers prepared by other methods, such as sol−gel coating.[3,7−9] We ascribed the unsatisfactory PEC enhancement to a low coverage of the ALD Al_2O_3 shell layers on the nanoporous TiO_2 electrodes as a result of that the island growth mode prevails during the ALD deposition. To further optimize the PCEs of DSSCs featuring Al_2O_3/TiO_2 electrodes, it will be necessary to know well the dependence of the coverage of the Al_2O_3 overlayers on the number of ALD deposition cycles. However, to correctly determine the coverage of an ultrathin Al_2O_3 layer coated on a porous electrode is difficult because there is presently no reliable analytical tool for the measurement. For instance, information provided by TEM analysis with an atomic scale resolution is limited to a localized area, and sample damage may occur during TEM sample preparations.

X-ray photoelectron spectroscopy (XPS) has a very small probe depth (<10 nm) and is often used to determine the coverage of an ultrathin film on a flat substrate in terms of measuring XPS signals of the substrate as a function of the amount of deposited film materials.[15,16] However, XPS becomes less straightforward when the coverage on a curved substrate, such as a particle, is studied. Theoretical models based on XPS to evaluate the coverage of an ultrathin layer on a particle usually requires an elaborate mathematical derivation with complex geometric considerations.[17,18] This is particularly so for ultrathin films deposited on porous substrates composed of interconnected nanoparticales. The purpose of this study is to develop a multilayer C/S model, using XPS, to measure the coverage of shell layers on the nanoporous electrodes of DSSCs. The model treats only the zenith angle in the mathematic derivation in terms of spherical symmetry considerations; therefore, the derivation is simpler compared with other models.[17−20] This model resembles more a real C/S material system as in the case of the porous TiO_2 electrode. Using these characterization techniques, we studied the influence of the coverage of the Al_2O_3 shell layers on the PCE of our DSSCs.

II. Theoretical Model

Like several previous reported models[17−20] that relate the adsorbate coverage on a spherical particle to the XPS signal emitted from the particle, the basic concept of our core/shell

* To whom correspondence should be addressed. E-mail: tien@itri.org.tw (T.-C.T.), fmpan@faculty.nctu.edu.tw (F.-M.P.).
† National Chiao Tung University.
‡ Industrial Technology Research Institute.
§ National Taiwan University.

10.1021/jp1023229
Published on Web 05/11/2010

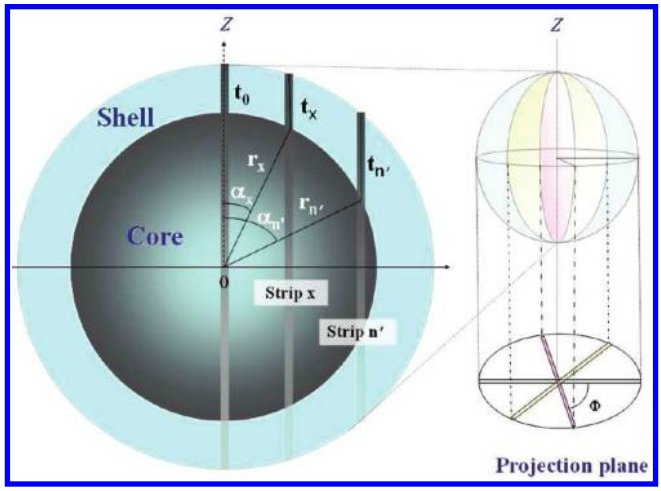

Figure 1. C/S model for calculating the fractional coverage (θ) of shell layers from an isolated C/S particle. The left circular plane is the cross-sectional plane that produces a projection line at a certain azimuth angle.

model divides the nanoparticle, which is assumed to be spherical, into many small partitions and considers separately the XPS signal emitted from each partition. In this model, numerous identical circular planes can be constructed from a sphere, as shown in Figure 1, in which the projections of three such circular planes at different azimuth angles (ϕ) are illustrated. The symmetrical geometry of the spherical particle allows us to exclude the participation of the ϕ angle in the derivation of the relation of the shell coverage with the XPS signal emitted from the core, thus only a circular plane at a fixed ϕ angle is taken into account to derive the relation. The circular plane is divided into 1000 strips with the long axis perpendicular to the sample surface. As shown in Figure 1, the thickness of the shell (t_x) in a strip, for example, strip x, depends on the strip angle (α_x) between the strip passing through the origin of the circle (O) and the line connecting point O with the intersecting point of strip x and the circle. Each strip is so thin that we may consider, within the strip, that the surface of the core particle is flat. Because the hemispherical energy analyzer is located from the sample at a distance much larger than the sample size, we assume that electrons emitted from all the strips have the same emission angle, which is 0° under the present analysis configuration.

In a previous study,[14] we found that ALD Al_2O_3 deposition on the porous TiO_2 electrode followed the island growth (Volmer−Weber) mode according to a plot of the growth per cycle versus the number of ALD reaction cycles. On the basis of Sitar's study,[16] the dependence of XPS signals of a flat substrate on the island coverage (θ_{island}) can be expressed as the following equation

$$I_s/I_0 = (1 - \theta_{island}) + \theta_{island} \times e^{-na/\lambda} \quad (1)$$

where I_s and I_0 are the intensities of photoelectrons emitted from the substrate with and without the thin film material, respectively, n is the number of monolayers in an island, a is the thickness of each monolayer, and λ is the inelastic mean free path (IMFP) of electrons traveling in the overlayer. Assuming a uniform coverage, we replace θ_{island} with the coverage of the shell material (fractional coverage, θ) on the two ends of each strip and introduce the strip angle (α_x) for the thickness calculation, and thus, eq 1 can be converted into the following expression

$$\Delta I/\Delta I_\alpha = (1 - \theta) + \theta \times e^{-t/(\lambda_{shell} \times \cos\alpha)} \quad (2)$$

where ΔI and ΔI_α are the intensities of photoelectrons emitted from a single strip with and without the shell layer, respectively, t is the thickness of the shell layer, α is the strip angle (θ values from 0° to 90°), and λ_{shell} is the inelastic mean free path (IMFP) of electrons traveling in the shell layer. We assume in this model that θ is the same for all the 1000 strips because of the homogeneous deposition nature of ALD. By summing up the values of ΔI of all strips in terms of α (from $\theta = 0°$ to $\theta = 90°$), we obtained an equation representing the total intensity (I) of photoelectrons emitted from the entire half part of the circular plane with the shell layer as follows:

$$I = \sum_{\alpha=0^\circ}^{90^\circ} \Delta I = \sum_{\alpha=0^\circ}^{90^\circ} \{\Delta I_\alpha \times [(1 - \theta) + \theta e^{-t/(\lambda_{shell} \times \cos\alpha)}]\} \quad (3)$$

The value of ΔI_α can be calculated using the following equation[20]

$$\Delta I_\alpha = \Delta I_{bulk} \times [1 - e^{(-2r\cos\alpha/\lambda_{core})}] \quad (4)$$

where ΔI_{bulk} represents the intensity of the photoelectrons from a strip of infinite length (relative to λ_{core}), r is the radius of the circular plane, and λ_{core} is the IMFP of electrons traveling in the core particle. In this study, the radius of the core particle is around 10 nm. Substituting eq 4 into eq 3, we obtain

$$I = \sum_{\alpha = 0^\circ}^{90^\circ} \{\Delta I_{bulk} \times [1 - e^{(-2r\cos\alpha/\lambda_{core})}] \times [(1 - \theta) + \theta e^{-t/(\lambda_{shell} \times \cos\alpha)}]\} \quad (5)$$

At the boundary conditions ($t = 0$, $\theta = 0$)

$$I = I_0 = \sum_{\alpha = 0^\circ}^{90^\circ} \{\Delta I_{bulk} \times [1 - e^{(-2r\cos\alpha/\lambda_{core})}]\} \quad (6)$$

where I_0 is the intensity of photoelectrons from the circular plane without the shell layers. Because ΔI_{bulk} is independent of angle α, eq 6 can be rewritten and converted into

$$\Delta I_{bulk} = I_0 \div \sum_{\alpha = 0^\circ}^{90^\circ} [1 - e^{(-2r\cos\alpha/\lambda_{core})}] \quad (7)$$

Substituting eq 7 into eq 5, we obtain

$$\frac{I}{I_0} = \sum_{\alpha = 0^\circ}^{90^\circ} \{[1 - e^{(-2r\cos\alpha/\lambda_{core})}] \times [(1 - \theta) + \theta e^{-t/(\lambda_{shell} \times \cos\alpha)}]\} \div \sum_{\alpha = 0^\circ}^{90^\circ} [1 - e^{(-2r\cos\alpha/\lambda_{core})}] \quad (8)$$

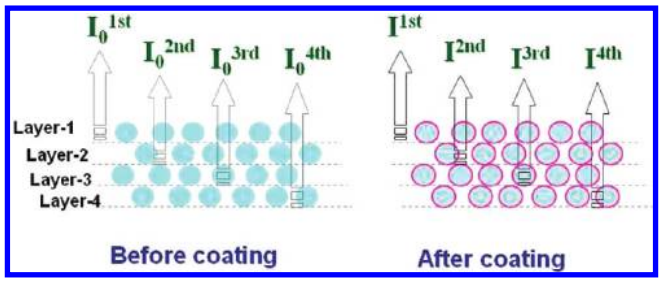

Figure 2. Multilayer C/S model for calculating the coverage of shell layers from each layer.

The values of λ_{core} and λ_{shell} (nm) can be calculated using eqs 9 and 10[21]

$$\lambda = 2170aE^{-2} + 0.72a^{3/2}E^{1/2} \quad (9)$$

$$a = \left(\frac{10^{27}M_W}{\rho n_A N_a}\right)^{1/3} \quad (10)$$

where E is the kinetic energy (eV) of the detected electron, M_W is the molecular weight of the core or shell material, ρ is the density, n_A is the number of the atoms in a molecule, and N_a is Avogadro's number. Although the I/I_0 ratio of eq 8 is derived for a single circular plane, it also equals to the XPS signal ratio of an entire core particle without and with the shell layer if homogeneous coverage is assumed, which is likely applicable to ALD deposition. This is because the model symmetrically divides a core particle into numerous identical circular planes.

Equation 8 is only good for the evaluation of the I/I_0 ratio for one C/S particle or samples with one monolayer of C/S particles. To study the relation of the I/I_0 ratio with the fractional coverage, θ, for a multilayer sample, such as the porous DSSC electrode composed of interconnected TiO_2/Al_2O_3 core shell nanoparticles, further modification for eq 8 is required. As shown in Figure 2, photoelectrons emitted from C/S particles below the first monolayer can still escape from the sample surface if open space is available or the upper layer is thinner than the escape depth of photoelectrons. The total XPS signal intensity of the C/S structured thin film with (I^{total}) and without (I_0^{total}) the shell layer can be expressed by the following equations

$$I_0^{total} = I_0^{1st} + I_0^{2nd} + I_0^{3rd} + I_0^{4th} + ... + I_0^{nth} \quad (11)$$

$$I^{total} = I^{1st} + I^{2nd} + I^{3rd} + I^{4th} + ... + I^{nth} \quad (12)$$

where I_0^{nth} and I^{nth} are the signal intensities of the nth layer before and after the shell coating, respectively (last n = total thickness of layers/2r). Because the derivation for the relation of the ratio of I^{total}/I_0^{total} with the fractional coverage is rather complex, we will present only the final result of the derivation. A detailed derivation is given in the Supporting Information. The I^{total}/I_0^{total} ratio can be related to the fractional coverage as follows

$$\frac{I^{total}}{I_0^{total}} = \frac{I}{I_0} \times \frac{1 + M + M^2 + M^3... + M^{n-1}}{1 + M(0) + [M(0)]^2 + [M(0)]^3... + [M(0)]^{n-1}} \quad (13)$$

where M is a function of θ, λ_{core}, λ_{shell}, and the radii of the core particle before and after the shell coating and $M(0)$ denotes M at $\theta = 0$.

Although the equations derived above are based on the concept of the escape depth of photoelectrons, eqs 8 and 13 are also applicable to Auger electrons, which have a similar inelastic scattering behavior in solids as photoelectrons. In this study, we use XPS to estimate the fractional coverage of ALD Al_2O_3 deposited on the porous electrode composed of interconnected TiO_2 nanoparticles in terms of eq 13 and study the dependence of the DSSC performance on the coverage of the Al_2O_3 shell layer.

III. Sample Fabrication

The layer structure of the DSSCs comprised a transparent, conductive glass/TiO_2 electrode featuring an optional Al_2O_3 layer coating of the bis(tetrabutylammonium) salt of *cis*-di(thiocyanato)-*N*,*N*-bis(2,2′-bipyridyl-4,4′-dicarboxylic acid)ruthenium(II) (N719 dye) and electrolyte/Pt/transparent conductive glass. The transparent conductive glass (Nippon Sheet Glass Co., Ltd.) contained a fluorine-doped oxide (FTO) film having a sheet resistance of 10−12 Ω/cm^2. The TiO_2 electrodes were 6 mm in diameter and composed of two screen-printed layers: a 12 μm thick nanoporous layer at the bottom (anatase layer) formed from ca. 20 nm diameter TiO_2 nanoparticles and a 4 μm thick porous layer at the top (rutile layer) formed from TiO_2 particles having sizes in the range of 200−400 nm. The ca. 20 nm diameter TiO_2 nanoparticles were prepared using a previously reported method;[22] they were identified (XRD) as having the anatase phase. The 200−400 nm diameter TiO_2 particles were purchased from DuPont (Ti-Pure R-706); they had an average size of ca. 300 nm and were the rutile phase (XRD). The titanium oxide film was annealed at 230 °C before the ALD Al_2O_3 deposition.

Atomic layers of Al_2O_3 were deposited on the TiO_2 electrodes using a Cambridge NanoTech Savannah 100 ALD system, with trimethylaluminum (TMA) and H_2O as precursors and a deposition temperature of 150 °C. The ALD process featured a given number of identical cycles, each containing the following six steps: dosing with H_2O for 0.05 s, soaking in the H_2O dose for 2 min, evacuation for 5 min, dosing with TMA by opening the TMA valve for 0.05 s, soaking in the TMA dose for 2 min, and evacuation for 5 min. After the precursors had been removed with a N_2 stream at a constant flow rate of 20 sccm, the chamber was closed for the subsequent soaking process. The TiO_2 electrodes prepared with and without the ALD Al_2O_3 overlayer were both sensitized with the N719 dye to saturation in a N_2 glovebox. The electrolyte solution comprised 0.1 M LiI, 0.03 M I_2, 0.5 M *tert*-butylpyridine, and 0.5 M 1,2-dimethyl-3-propylimidazoliumiodide (PrMeImI) in anhydrous acetonitrile.

The photocurrent−voltage characteristics of the DSSCs were measured under AM 1.5G illumination simulated with a Peccell solar simulator. The TiO_2 electrodes were analyzed using a field emission transmission electron microscope (TEM) (JEOL, JEM-2100f) operated at a 0.1 nm lattice resolution. XPS and Auger electron spectroscopy (AES) analyses of the TiO_2 electrode were performed using VG ESCAlab 250 and VG MicroLab 350 electron spectroscopes operated at a base pressure of 1×10^{-10} Torr, using the Al Kα beam (hv = 1486.6 eV) for XPS and a 5 keV electron beam for AES. The energy resolution in the XPS spectra was 25 meV, as suggested by the instrument manufacturer.

The high-resolution TEM (HRTEM) image in Figure 3a displays the nanocrystalline TiO_2 core particles prepared without

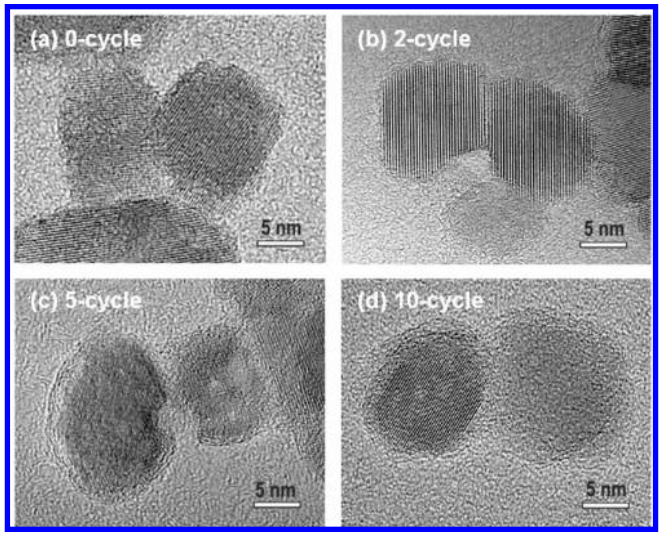

Figure 3. TEM images of nanocrystalline TiO_2 core particles prepared (a) without an Al_2O_3 shell layer, (b) with a two-cycle ALD Al_2O_3 shell layer, (c) with a five-cycle ALD Al_2O_3 shell layer, and (d) with a 10-cycle ALD Al_2O_3 shell layer.

the Al_2O_3 shell layer; Figure 3b−d presents HRTEM images of the crystalline TiO_2 particles prepared with Al_2O_3 shell layers using 2 to 10 cycles of ALD. All of the samples featured spherical-like, uniform, interconnected TiO_2 particles that were ca. 20 nm in size. Table 1 lists the thicknesses of the Al_2O_3 overlayers prepared using 1 to 30 ALD cycles, as determined by TEM. Each listed thickness is the average value of 10 thickness measurements for the Al_2O_3 overlayer. The thickness values indicate a significant discrepancy in the deposition rates (nanometers/cycle) for the various reaction cycles. For a layer-by-layer growth process, a rate of deposition equivalent to 1 ML of the film per ALD cycle is ideal, that is, ∼0.18 nm/cycle for Al_2O_3.[23] To better examine the distribution of the ALD Al_2O_3 deposit on the anatase nanoparticles, Figure 4 shows HRTEM images of the shell material deposited on a local area of the core particles before and after the first and the fifth deposition cycles. The HRTEM images clearly show that the distribution of the ALD Al_2O_3 deposit is not uniform on the core particles, indicating that the ALD deposition is via an island growth process.

IV. Applications of the C/S Model on the Nanoporous Electrode of DSSCs

Figure 5 shows the Ti $2p_{3/2}$ XPS spectrum of the as-received TiO_2 electrodes, indicating that the Ti $2p_{3/2}$ core level of the nanoporous TiO_2 electrodes was located at 458.9 eV, that is, within the range from 458.8 to 459.4 eV reported for TiO_2 in the literature.[24] Following ALD of the first Al_2O_3 overlayer, the binding energy of the Ti $2p_{3/2}$ core level of the TiO_2 layers shifted by −0.5 to 458.4 eV; after 30 cycles, it shifted by +0.5 to 458.9 eV. These shifts in the Ti $2p_{3/2}$ core levels indicate that the Ti−O bond strength decreased within the 0.2 nm thick Al_2O_3 shell layer. The binding energy shift of the Ti $2p_{3/2}$ electron from −0.5 to +0.5 eV with increasing the thickness of the Al_2O_3 overlayers can be partly attributed to the change in the work function of the Al_2O_3−TiO_2 electrode. According to our previous study, the work function (WF) of the electrode increases from 4.7 to 5.1 eV after the first ALD cycle, followed by decreasing with increasing the thickness of the Al_2O_3 overlayers (4.3 eV after 10 cycles of ALD).[14] The magnitude and direction of the core level shifts observed in the XPS spectra are in good agreement with the change of the WF with increasing the thickness of the Al_2O_3 overlayer.

Figure 6 displays the I^{total}/I_0^{total} ratio measured by XPS as a function of the thickness of the Al_2O_3 shell layer on the TiO_2 electrode. Each datum of the I^{total}/I_0^{total} ratio is the average value of five measurements, with a deviation smaller than 3%. The solid curves are the theoretical curves, derived from the C/S model, for the I^{total}/I_0^{total} ratio as a function of the shell thickness at various coverages (θ). When the number of ALD reaction cycles is smaller than 15, the measured I^{total}/I_0^{total} ratio falls on the curves for $\theta < 1$, revealing the presence of bare TiO_2 surface areas. This is in agreement with the HRTEM images shown in Figure 4, which show an uneven distribution of the ALD Al_2O_3 deposits on the TiO_2 nanoparticles and suggests that the deposition of the ALD Al_2O_3 film on TiO_2 nanoparticles is via the island growth mode. For an island film growth, the growth and coalescence of deposited islands proceed during the ALD reaction, and a continuous island film will eventually develop. According to Figure 6, the measured I^{total}/I_0^{total} ratios for the shell layers deposited by more than 15 reaction cycles fall on the curve for $\theta = 1$, indicating that the nanoporous TiO_2 electrode was completely covered by the Al_2O_3 shell layer; that is, a continuous Al_2O_3 film is formed.

Because XPS is very surface-sensitive with the probe depth smaller than 10 nm, a conclusive determination of the I^{total}/I_0^{total} ratio through the 12 μm thick porous TiO_2 thin film electrode simply by the XPS analysis is questionable. To clarify this issue, we used AES to analyze the cross section of a 22 μm thick nanoporous TiO_2 layer with 10 cycles of the ALD Al_2O_3 overlayer. The AES analysis showed that the variation of the Al(KLL) signal was less than 1.8% through the cross section, suggesting that the ALD Al_2O_3 layer was evenly deposited inside the porous electrode. This result suggests that using XPS to study the Al_2O_3 coverage on the nanoporous electrodes of DSSCs in terms of the C/S model is justified.

According to Figure 6, the ALD deposition with 1, 2, 5, and 10 cycles results in an Al_2O_3 coverage of 0.25, 0.40, 0.71 and 0.83, respectively. However, the fitted coverage values are likely to have significant deviations from the true values because of several limitations bound to the application of the C/S model to the nanoporous DSSC electrodes. First, the C/S model assumes that the particle has a spherical shape, but the TiO_2 nanoparticles in the DSSC electrodes exhibit various rounding shapes, which are far from a perfect spherical geometry. Second, the C/S model considers only those photoelectrons emitting from nanoparticles in the direction perpendicular to the sample surface. Although the line of sight of the input lens of the electron energy analyzer is perpendicular to the sample surface and the distance between the sample and the input aperture is considered to be infinitive compared with the nanoparticle diameter, detection of stray electrons emitting from other emission angles by the analyzer is inevitable. Third, the C/S model assumes a uniform island growth during the film deposition; that is, all islands developing on the substrate have the same thickness. However, this seems not to be true for the case of ALD Al_2O_3 deposition on TiO_2 nanoparticles according to the TEM analysis. Each datum shown in Figure 6 is the average value of 10 thickness measurements, and the average thickness will certainly deviate from the theoretical value for a particular coverage. Despite the above-described limitations of the C/S model, Figure 6 shows a reasonable trend in the coverage increase upon the increase in the number of ALD cycles. Therefore, we believe that the C/S model is applicable in the evaluation of the ALD Al_2O_3 coverage.

TABLE 1: Thickness and Deposition Rate of the ALD Al_2O_3 Shell Layers on TiO_2 Electrodes

sample: Al_2O_3 shell layers	0-cycle	1-cycle	2-cycle	5-cycle	10-cycle	15-cycle	20-cycle	30-cycle
thickness (nm)[a]	0	0.2 ± 0.1	0.5 ± 0.2	1 ± 0.4	1.9 ± 0.3	2.5 ± 0.4	2.8 ± 0.5	4.5 ± 0.5
deposition rate (nm/cycle)		0.2 ± 0.1	0.25 ± 0.1	0.2 ± 0.08	0.19 ± 0.03	0.17 ± 0.02	0.14 ± 0.02	0.15 ± 0.02

[a] The thickness listed in the table is the average value of 10 TEM measurements at different locations of the C/S nanoparticle.

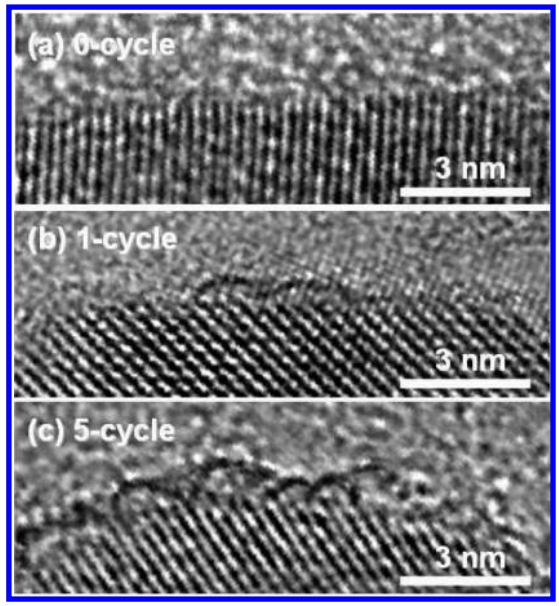

Figure 4. Enlarged TEM images show the TiO_2 core particles (a) without an Al_2O_3 shell layer, (b) with a one-cycle ALD Al_2O_3 shell layer, and (c) with a five-cycle ALD Al_2O_3 shell layer.

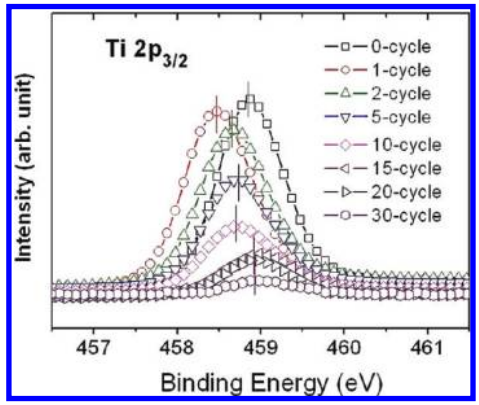

Figure 5. XPS spectra of the Ti $2p_{3/2}$ peaks from the nanoporous TiO_2 electrodes.

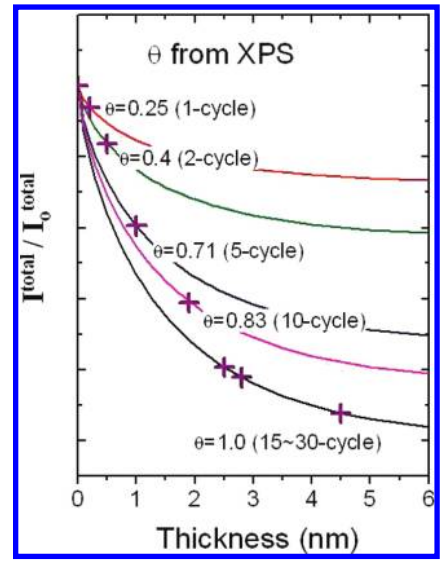

Figure 6. Coverages (θ) of Al_2O_3 shell layers on TiO_2 electrodes, obtained from XPS analyses. The experimental data (crosses) match the corresponding theoretical curves from our C/S model.

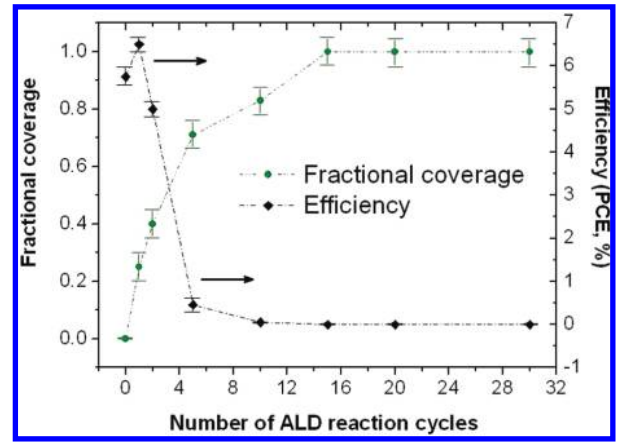

Figure 7. Changes in the PCE and coverage, plotted with respect to the number of ALD reaction cycles for Al_2O_3 shell layers on TiO_2 electrodes.

Figure 7 shows that the PCEs of the DSSCs changed upon varying the number of ALD reaction cycles of the Al_2O_3 shell layers. Each PCE datum in the figure is the average efficiency of 20 solar cells. Table 2 indicates that the efficiency increased initially by ~13% at an Al_2O_3 layer thickness of ca. 0.2 nm, but then it dropped dramatically to almost 0% upon further increasing the thickness. The initial increase of J_{sc} at an ~0.2 nm thickness of the Al_2O_3 layer may be attributed, in part, to the reduction of recombination.[3,6−9] On the other hand, the drop of the PCE is likely due to the tunneling effect,[25] which will exponentially decrease the current from dye to TiO_2 electrode with increasing the thickness of the Al_2O_3 overlayer, as indicated by the short-circuit current (J_{sc}) listed in Table 2. The initial increase in the value of the V_{oc} is suggested to result from that the high work function of the optimal ALD Al_2O_3 layer thickness, as discussed above, provided a positive built-in potential (eV_{bi}) at the Al_2O_3−TiO_2 interface.[14] Thus, increasing the coverage of the optimal ALD Al_2O_3 overlayer on the nanoporous TiO_2 electrodes should enhance the PCE proportionally.

TABLE 2: Cell Performance of DSSCs Containing ALD Al_2O_3 Overlayers of Various Thicknesses

Al_2O_3 thickness (nm)	V_{oc} (mV)	J_{sc} (mA/cm^2)	FF (%)	PCE (%)
0	737 ± 9	11.57 ± 0.43	66.9 ± 0.7	5.75 ± 0.22
0.2 (1-cycle)	765 ± 9	12.46 ± 0.38	68.7 ± 0.8	6.50 ± 0.15
0.5 (2-cycle)	744 ± 38	9.77 ± 0.21	68.6 ± 5.8	5.00 ± 0.16
1.0 (5-cycle)	796 ± 4	0.86 ± 0.11	67.9 ± 8.8	0.46 ± 0.12
1.9 (10-cycle)	764 ± 104	0.18 ± 0.01	37.2 ± 3.4	0.05 ± 0.01

The optimal ALD Al_2O_3 layer thickness is 1 ML, or 0.2 nm, which is considerably thinner than the reported 0.9−2.5 nm thicknesses of Al_2O_3 films derived using sol−gel techniques.[9,26] As discussed in previous studies,[26,27] the thickness of the sol−gel

films can only be altered with a resolution down to ~1 nm; that is, the minimum achievable Al_2O_3 thickness is ca. 1 nm. The poorer infiltrating ability of the liquid precursors during sol−gel processing, generally resulting in an overestimation of the Al_2O_3 thickness (i.e., the sol−gel films may accidentally be thinner, falling into the desirable range of Al_2O_3 layer thicknesses on electrode surfaces that are more difficult for the precursors to reach). Nevertheless, the ALD approach may not have much of an advantage over high-temperature sol−gel techniques due, in part, to the low coverage of ALD Al_2O_3 overlayers on nanoporous TiO_2 electrodes at the optimal overlayer thickness. Ideally, at the optimal thickness of the ALD Al_2O_3 overlayer, the PCE of the electrode is proportional to the fractional coverage of the overlayer. According to Figure 7 and Table 2, the PCE is improved from 5.75% to 6.50% (i.e., an enhancement of 13.0%) if the nanoporous TiO_2 electrode is coated by the Al_2O_3 overlayer with a coverage of 0.25. Accordingly, as the coverage of the Al_2O_3 overlayer approaches 1, the PCE of the electrode would have a PCE enhancement of more than 52%. However, under the present ALD deposition condition, the high PCE enhancement cannot be realized because of the island growth mode. If optimal ALD deposition conditions, such as the substrate temperature and precursor flow rate, can be successfully selected to increase the coverage for the first ALD deposition cycle, we believe that a better PCE for the ALD Al_2O_3−TiO_2 C/S DSSCs is achievable.

V. Conclusions

In this study, we established a C/S model, using XPS electron spectroscopy data, to calculate the surface coverage of shell layers. A relation of the XPS signal of a nanoporous substrate featuring interconnected nanoparticles with the fractional coverage of the shell layer on the nanoparticles can be extracted from the model. We used the model to estimate the coverage of the ALD Al_2O_3 shell layer deposited on the nanoporous TiO_2 electrodes of DSSCs as a function of the number of ALD reaction cycles. The coverage increased from 0.25 to 1.0 upon increasing the thickness of the Al_2O_3 shell layers, indicating that the ALD Al_2O_3 deposition on the nanoporous electrode was via the island growth mode. The PCE of the DSSCs was highest after the first ALD reaction cycle for the Al_2O_3 shell layers. On the basis of the coverage analysis, we predict that an improvement in the PCE of ~50% is obtainable when a single monolayer of ALD Al_2O_3 (i.e., at the coverage of 1.0) is deposited on the nanoporous TiO_2 electrode.

Acknowledgment. We thank Chia-Hua Lee (ITRI, Taiwan), Su-Jen Chen (ITRI, Taiwan), Iva Chan (ITRI, Taiwan), Peter Glink (www.editchem.com, U.S.A.), and the Microstructure and Characterization Laboratory (ITRI, Taiwan) for technical assistance and the Ministry of Economic Affairs of Taiwan, ROC, for generous financial assistance.

Supporting Information Available: The derivation on the total XPS/AES signal intensity of the core−shell (C/S) structured nanoporous film with and without the shell layer is presented in the Supporting Information. This material is available free of charge via the Internet at http://pubs.acs.org.

References and Notes

(1) Cui, Y.; Liu, L.; Li, B.; Zhou, X.; Xu, N. *J. Phys. Chem. C* **2010**, *114*, 2434.
(2) Antony, J.; Nutting, J.; Baer, D. R.; Meyer, D.; Sharma, A.; Qiang, Y. *J. Nanomater.* **2006**, 54961.
(3) Zaban, A.; Chen, S. G.; Chappel, S.; Gregg, B. A. *Chem. Commun.* **2000**, 2231.
(4) Kamat, P. V.; Schatz, G. C. *J. Phys. Chem. C* **2009**, *113*, 15473.
(5) Rowley, J.; Meyer, G. J. *J. Phys. Chem. C* **2009**, *113*, 18444.
(6) Lin, C.; Tsai, F. Y.; Lee, M. H.; Lee, C. H.; Tien, T. C.; Wang, L. P.; Tsai, S. Y. *J. Mater. Chem.* **2009**, *19*, 2999.
(7) Chen, S. G.; Chappel, S.; Diamant, Y.; Zaban, A. *Chem. Mater.* **2001**, *13*, 4629.
(8) Chappel, S.; Chen, S. G.; Zaban, A. *Langmuir* **2002**, *18*, 3336.
(9) Palomares, E.; Clifford, J. N.; Haque, S. A.; Lutz, T.; Durrant, J. R. *J. Am. Chem. Soc.* **2003**, *125*, 475.
(10) Zhang, X. T.; Liu, H. W.; Taguchi, T.; Meng, Q. B.; Sato, O.; Fujishima, A. *Sol. Energy Mater. Sol. Cells* **2004**, *81*, 197.
(11) Liu, Z.; Pan, K.; Liu, M.; Wang, M.; Lu, Q.; Li, J.; Bai, Y.; Li, T. *Electrochim. Acta* **2005**, *50*, 2583.
(12) Guo, J.; She, C.; Lian, T. *J. Phys. Chem. C* **2007**, *111*, 8979.
(13) Kim, W.; Tachikawa, T.; Majima, T.; Choi, W. *J. Phys. Chem. C* **2009**, *113*, 10603.
(14) Tien, T. C.; Pan, F. M.; Wang, L. P.; Lee, C. H.; Tung, Y. L.; Tsai, S. Y.; Lin, C.; Tsai, F. Y.; Chen, S. J. *Nanotechnology* **2009**, *20*, 305201.
(15) Hartlieb, P. J.; Roskowski, A.; Davis, R. F.; Plattow, W.; Nemanich, R. J. *J. Appl. Phys.* **2002**, *91*, 732.
(16) Sitar, Z.; Smith, L. L.; Davis, R. F. *J. Cryst. Growth* **1994**, *141*, 11.
(17) Gillet, J. N.; Meunier, M. *J. Phys. Chem. B* **2005**, *109*, 8733.
(18) Martin, J. E.; Herzing, A. A.; Yan, W.; Li, X. Q.; Kobel, B. E.; Kiely, C. J.; Zhang, W. X. *Langmuir* **2008**, *24*, 4329.
(19) Renault, O.; Marlier, R.; Barrrett, N. T.; Martinez, E.; Baron, T.; Gely, M.; De Salvo, B. *Surf. Interface Anal.* **2006**, *38*, 486.
(20) Mohai, M.; Bertoti, I. *Surf. Interface Anal.* **2004**, *36*, 805.
(21) Tanuma, S.; Powell, C. J.; Penn, D. R. *Surf. Interface Anal.* **1988**, *11*, 577.
(22) Zaban, A.; Ferrere, S.; Sprague, J.; Gregg, B. A. *J. Phys. Chem. B* **1997**, *101*, 55.
(23) Gosset, L. G.; Damlencourt, J. F.; Renault, O.; Rouchon, D.; Holliger, P.; Ermolieff, A.; Trimaille, I.; Ganem, J. J.; Martin, F.; Semeria, M. N. *J. Non-Cryst. Solids* **2002**, *303*, 17.
(24) Moulder, J. F.; Stickle, W. F.; Sobol, P. E.; Bomben, K. D. *Handbook of X-ray Photoelectron Spectroscopy*; Perkin-Elmer Press: Eden Prairie, MN, 1962; pp 45−73.
(25) Sze, S. M. *Physics of Semiconductor Devices*; John Wiley & Sons: New York, 1983; Vol. 97.
(26) Palomares, E.; Clifford, J. N.; Haque, S. A.; Lutz, T.; Durrant, J. R. *Chem. Commun.* **2002**, 1464.
(27) Bandaranayake, K. M. P.; Indika Senevirathna, M. K.; Prasad Weligamuwa, P. M. G. M.; Tennakone, K. *Coord. Chem. Rev.* **2004**, *248*, 1277.

JP1023229